ROGUE WAVES IN THE AGULHAS REGION

G C Hocking*

Industry Representative

M M Matabane†

Study Group Participants

Emma Nel, Samah Ali, Salma Ahmedai, Alice Markham, Katlego Sebogodi, Nyathi Freeman, Hloniphile Sithole Mthethwa, Morwakoma Matabane, Ndivhuwo Ndou, Franco du Plessis, Thama Duba, Graeme Hocking, Erick Mubai

Abstract

Rogue Waves are large waves that appear "out of nowhere" in the open ocean and in near-shore waters. The Mathematics in Industry Study Group considered these waves due to their frequency at locations off the South African coast. The group took multiple approaches to consider this problem. There are a number of quite sophisticated models of these waves, but in this work we try to reproduce something like a rogue wave with a very simple free surface model. The results indicate that such a model can produce something that approaches the form of a rogue wave. In addition, data in regions off the South African coast were considered with a view to determining under what conditions such waves are most prevalent, and a simple model of current interactions around the South African coast was proposed. A review of literature identified a very important paper providing analyses of data for a large collection of real data.

Tools: Partial Differential Equations, Perturbation techniques, Fourier Series

Keywords: Water Waves, wave heights, ocean currents, ocean bottom topography, wave data

*School of Mathematics and Statistics, Murdoch University, Perth, Western Australia, Australia. *email: g.hocking@ murdoch.edu.au*

†South African Weather Service, Centurion, Pretoria. *email: Morwakoma.Matabane@weathersa.co.za*

1 Introduction

A high frequency of rogue or freak waves have recently been measured around the South African coast, especially in the Agulhas region (off the south-east coast of South Africa). Some have resulted in loss of life or livelihood, flooding, and damage to infrastructure. The group was asked to look at the generation and cause of rogue waves in particular related to this region. Rogue waves have a formal definition of having a peak height of double the significant wave height, defined as the average height of the highest one third of waves over the relevant period. The main danger is that they seem to appear with no warning, "out of nowhere".

There are a large number of papers speculating on the nature and propagation of rogue waves, but most do not examine the origins of such waves. A paper of particular importance to this problem is that of Christou and Ewans [1], who examined existing data from a number of locations around the world. These data were taken from oil platforms and other ocean-based situations. The result was a comprehensive analysis of 122 million waves collected from reliable and verifiable sources. They found around 3649 rogue waves, and these were analysed together with regular ocean waves. Thus they found that only one in every 30,000 waves might be a rogue wave. While this sounds like a very small number, it must be remembered that ocean waves have a period of only several seconds, so at any given location there might be approximately one such wave every two or three days on average. They drew the following conclusions from their detailed analyses;

- A rogue wave is generally steeper than normal waves but not all steep waves are "rogue",
- The average rogue wave shape had higher crests and deeper troughs than the highest 1% of normal waves,
- Rogue waves were slightly more narrow-banded than the highest 1% of normal waves,
- The rogue wave samples exhibit dispersive focusing, resulting in the majority of frequency components coming into phase with each other at the time of the rogue wave events,
- The study presented evidence to suggest that rogue waves are extraordinary and rare occurrences, but still a part of the normal population, and that they are caused by dispersive focusing.

There is a large amount of literature that discusses the possibility that rogue waves are examples of solitons or solitary waves. Solitons are known to propagate long distances with minimal attenuation, and it is this property that makes them dangerous. The equations involved are the Korteweg-de Vries [4, 6] equation and the nonlinear Schrödinger equation [3]. These equations assume waves have a long wavelength compared to the depth of the water. An earlier report at the South African Study Group [5] considered these models in more detail and presented simulations of the generation of solitons as the ocean current flowed over a step in the ocean floor, and so we do not repeat that work here.

This modelling using equations derived from fluid dynamics to consider the generation of such waves specific to local conditions is one approach. An alternative is to determine the likelihood of rogue waves in a particular location using data analysis, taking into account weather, sea state and bottom topography. The group used both of these approaches and their outcomes are described in what follows.

One part of the group set out to create a simple model of the currents around the southern part of South Africa, including the gulf stream, the Agulhas current and the main Southern Ocean easterly current. This model currently includes no topography but it is hoped that future work might incorporate it so that a simplified wave-height model might be developed. This is discussed in section 3. Another part of the group adopted a data-analytic approach and focused on the available meteorological, wave and ocean surface data for the region. However, in the time available the acquisition of data proved very difficult and so this component is limited to a suggested procedure. This work is presented in section 4.

To consider the effectiveness of a simple model, the group decided to attempt to simulate the large model study done at the University of Edinburgh [7], in which a circular wave tank, twenty five metres in diameter, was used to generate a wave with the same properties as a rogue wave. This was motivated in part by the conclusions of Christou and Ewans [1], who found that the waves consisted of waves combined by dispersive forcing. A linearised model of the free surface hydrodynamic equations was solved in polar coordinates and a spike in the center of the basin suggested that it would be possible to generate such a wave by the focusing of incoming waves. This model was then extended to include nonlinear effects. These results indicate that a focusing or convergence of the waves is a possible generating mechanism for rogue waves. This model is described in section 2.

2 A model of the wave tank experiment

The question of how difficult it might be to generate a wave with rogue wave like properties was considered by McAllister et. al. [7] who used a large circular basin with the facility to generate waves from all sides to recreate the famous Draupner rogue wave [2] that was recorded in the North Sea in 1995.

Here we consider a model that assumes an axisymmetric free surface flow generated in a circular basin to see if we can approximate their solution. The axisymmetric, unsteady, irrotational flow of an inviscid, incompressible, fluid of finite depth in a circular tank beneath a free surface is considered when a wave is transmitted inwards. The assumption of radial symmetry means the problem can be reduced to finding the free surface profile as a function of radial distance from the origin.

Consider a fluid beneath a free surface with initial depth H in a circular domain of radius $\hat{R}$. The bottom of the tank is at $\hat{z} = 0$. We can define a velocity potential $\Phi(\hat{r}, \hat{z}, \tau)$

such that $\hat{\mathbf{v}} = \nabla\Phi$ is the velocity vector for the flow in axisymmetric polar coordinates, and satisfies

$$\nabla^2\Phi = \Phi_{\hat{r}\hat{r}} + \frac{1}{\hat{r}}\Phi_{\hat{r}} + \Phi_{\hat{z}\hat{z}} = 0, \quad 0 < \hat{z} < N(\hat{r},\tau),\ 0 < \hat{r} < \hat{R}, \tau > 0$$

throughout the fluid domain where $\hat{z} = N(\hat{r},\tau)$ is the equation of the free surface. A solid, horizontal boundary at depth $\hat{z} = 0$ requires that $\Phi_z(\hat{r},0,\tau) = 0$ on $\hat{z} = 0$ and the vertical boundary at $\hat{r} = \hat{R}$ requires that $\Phi_r(\hat{r},\hat{z},\tau) = 0$.

The conditions on the free surface are the dynamic condition of atmospheric pressure on the free surface, which comes from the Bernoulli equation

$$\Phi_\tau + \frac{1}{2}(\hat{u}^2 + \hat{v}^2) + gN = 0 \ \text{ on } \quad \hat{z} = N(\hat{r},\tau) \tag{1}$$

and the kinematic condition,

$$N_\tau + \Phi_{\hat{r}}N_{\hat{r}} - \Phi_{\hat{z}} = 0 \quad \text{on} \quad \hat{z} = N(\hat{r},\tau). \tag{2}$$

Scaling depth with H and velocity with some quantity $U = H/T$ for a typical time T, we find the dimensionless equations are then

$$\nabla^2\phi = \phi_{rr} + \frac{1}{r}\phi_r + \phi_{zz} = 0, \quad 0 < z < \eta(r,t), \quad 0 < r < R, t > 0 \tag{3}$$

where $\mathbf{v} = \nabla\phi$ subject to

$$\phi_t + \frac{1}{2}(u^2 + v^2) + \eta = 0 \quad \text{on} \quad z = \eta(r,t), \tag{4}$$

and

$$\eta_t + \phi_r\eta_r - \phi_z = 0 \quad \text{on} \quad z = \eta(r,t), \tag{5}$$

while on the base it is required that

$$\phi_z(r,0,t) = 0 \quad \text{on} \quad z = 0, \tag{6}$$

Here R is the dimensionless radius of the tank and $z = \eta(r,t)$ is the elevation of the free surface and the nondimensional depth is one unit. There is also a condition of no flow through the boundary of the tank at $r = R$, and this can be written as

$$\phi_r(R,z,t) = 0, \qquad \text{on } r = R. \tag{7}$$

The initial conditions are that the flow is initiated from a quiescent situation and that the location of the free surface is known at $t = 0$ so that

$$\phi(r,z,0) = 0 \text{ on } z = \eta(r,0) \text{ and } \eta(r,0) = f(r). \tag{8}$$

where $f(r)$ is the initial elevation of the surface. We will pile up fluid near the outer boundary and then allow it to flow inwards.

2.1 The linear problem

The linearized problem is obtained by assuming that $\mathbf{v}$ and η are small quantities, so that product terms can be neglected. The surface equations are then evaluated on $z = 1$ (rather than $z = \eta(r, t)$, which would make the problem nonlinear).

Therefore, we seek a solution to Laplace's equation (3) with the linearized conditions on the free surface, which are

$$\begin{aligned} \eta_t &= \phi_z \text{ and } \phi_t = -\eta \text{ on } z = 1 \\ &\Rightarrow \phi_{tt} + \phi_z = 0 \quad \text{ on } z = 1, \end{aligned} \tag{9}$$

while on the bottom,

$$\phi_z(r, 0, t) = 0 \text{ on } z = 0. \tag{10}$$

and on the outer boundary

$$\phi_r(R, z, t) = 0 \text{ on } r = R. \tag{11}$$

We choose a form that satisfies the equation (3) and the boundary conditions (10) and (11), that is,

$$\phi(r, z, t) = \sum_{k=0}^{\infty} a_k(t) \cosh(\lambda_k z) J_0(\lambda_k r) \tag{12}$$

where J_0 is the first-kind Bessel function of order 0, and $\lambda_k,\ k = 0, 1, 2, \ldots$ are the eigenvalues of J_1, the first-kind Bessel function of order 1, since $J_0'(\lambda_k r) = -\lambda_k J_1(\lambda_k r), k = 0, 1, 2, \ldots$.

This choice (12) satisfies Laplace's equation 3 in polar coordinates, and the choice of λ_k satisfies equation (11), while the $\cosh \lambda_k z$ term has the property that condition (10) is satisfied. Thus it remains to satisfy (9).

Substituting (12) into (9), after some work we find that on $z = 1$,

$$\sum_{k=0}^{\infty} \left(a_k''(t) \cosh \lambda_k + a(k, t)\lambda_k \sinh \lambda_k\right) J_0(\lambda_k r) = 0 \tag{13}$$

where dashes refer to differentiation with respect to time. Thence the general problem for $a_k(t), k = 0, 1, 2, \ldots$ is

$$a_k''(t) \cosh \lambda_k + a_k \lambda_k \sinh \lambda_k = 0 \tag{14}$$

to which the general solution is (noting that the derivatives are with respect to t only),

$$a_k(t) = D_k \sin \omega_k t + C_k \cos \omega_k t \tag{15}$$

where

$$\omega_k = \sqrt{\lambda_k \tanh \lambda_k} \tag{16}$$

and C_k and D_k are constants to be determined. The value of $\omega_k, k = 0, 1, 2, \ldots$ provides a kind of dispersion relation for the waves of different wavenumber.

Thus the general solution for ϕ is

$$\phi(r,z,t) = \sum_{k=0}^{\infty} (D_k \sin \omega_k t + C_k \cos \omega_k t) \cosh(\lambda_k z) J_0(\lambda_k r) \tag{17}$$

In order to determine the form of D_k and C_k we must employ the initial conditions. From equations (9), we note that

$$\phi_t(r,1,0) = -\eta(r,0), \tag{18}$$

evaluated on $z = 1$, and so if $\eta(r,0) = f(r)$, we find at $t = 0$

$$\phi_t(r,1,0) = \sum_{k=0}^{\infty} D_k \omega_k J_0(\lambda_k r) = -f(r). \tag{19}$$

Another condition is required to find C_k and we choose $\phi(r,1,0) = 0$ for simplicity, which gives $C_k = 0, k = 0,1,2,\ldots$. Now we have a solution for any initial condition. Once D_k is determined via the orthogonality of eigenfunctions, equation (9) provides that $\eta = -\phi_t$ for all time, so

$$\eta(r,t) = -\phi_t(r,1,t) = -\sum_{k=0}^{\infty} D_k \omega_k \cos(\omega_k t) \cosh(\lambda_k) J_0(\lambda_k r) \tag{20}$$

where D_k is

$$\begin{aligned} D_k &= \frac{\int_0^R f(r) J_0(\lambda_k) r\,dr}{\int_0^R J_0^2(\lambda_k r) r\,dr}, \quad k = 0,1,2,\ldots \\ &= \frac{\int_0^R f(r) J_0(\lambda_k r) r\,dr}{\frac{R^2}{2} J_0^2(\lambda_k R)}, \quad k = 0,1,2,\ldots \end{aligned}$$

2.2 The full nonlinear problem

The linearised equations are only valid for small values of disturbance and velocities, and so to consider the full problem we need to solve the nonlinear version of the equations (3-8).

Again, we choose a form for $\phi(x,z,t)$ that satisfies the field equation (3) and the boundary conditions at $r = R$ and $z = 0$, i.e.

$$\phi(r,z,t) = a_0(t) + \sum_{k=1}^{\infty} a_k(t) \cosh(\lambda_k z) J_0(\lambda_k r), \tag{21}$$

and for $\eta(r,t)$ we choose the compatible form (see 21) to be

$$\eta(r,t) = b_0(t) + \sum_{k=1}^{\infty} b_k(t) J_0(\lambda_k r) \tag{22}$$

where the coefficients $a_k(t)$ and $b_k(t), k = 0, 1, 2, \dots$ are to be determined.

Whereas in the linear case, all quantities were calculated on the line $z = 1$, we must now do the computations on $z = \eta(r, t)$, partially invalidating orthogonality as a tool. Therefore we must solve the problem numerically, and the manner of that solution is to derive a set of first order differential equations for the $a_k(t)$ and $b_k(t)$, $k = 0, 1, 2, \dots$. For example, knowing that our choice for ϕ satisfies all boundary conditions we only need apply it on the free surface. Substituting (21) into (4) and (5) and then multiplying all by $rJ_0(\lambda_j r)$ and integrating from 0 to R, we obtain

$$b_0'(t) = \frac{2}{R^2}\int_0^R \left[\phi_z(r,\eta,t) - \phi_r(r,\eta,t)\eta_r\right] rdr, \tag{23}$$

$$b_k'(t) = \frac{2\int_0^R \left[\phi_z(r,\eta,t) - \phi_r(r,\eta,t)\eta_r\right] J_0(\lambda_k r) rdr}{R^2 J_0^2(\lambda_k R)}, \quad k = 1, 2, 3, \dots \tag{24}$$

$$\begin{aligned} a_0'(t)\frac{R^2}{2} + \sum_{k=1}^{\infty}\int_0^R a_k'(t)\cosh(\lambda_k\eta)J_0(\lambda_k r)rdr & \\ = -\int_0^R \eta r dr - \int_0^R \left[\frac{1}{2}(\phi_r^2 + \phi_z^2)\right] rdr & \\ = -b_0(t)\frac{R^2}{2} - \int_0^R \left[\frac{1}{2}(\phi_r^2 + \phi_z^2)\right] rdr & \qquad (25) \end{aligned}$$

$$\begin{aligned} [A_{kj}a_k'(t)] &= -\int_0^R \left[\frac{1}{2}(\phi_r^2 + \phi_z^2) + \eta\right] J_0(\lambda_k r)rdr, \\ &= -b_k(t)\frac{R^2}{2}J_0^2(\lambda_k R) - \int_0^R \left[\frac{1}{2}(\phi_r^2 + \phi_z^2)\right] J_0(\lambda_k r)rdr, \quad k = 1, 2, 3, \dots \qquad (26) \end{aligned}$$

where $A_{kj} = \int_0^R \cosh(\lambda_k\eta)J_0(\lambda_k r)J_0(\lambda_j r)rdr$ and (26) is therefore a matrix equation. The integrals can all be computed to high accuracy using Gaussian quadrature. The series' are truncated to N terms, and this provides $2N$ first-order differential equations for the coefficients $a_k(t), b_k(t)$, $k = 0, 1, 2, \dots, N-1$ and we can step forward in time using any DE solver (e.g. `ode45` in *Matlab* or `lsode` in *Octave*).

2.3 Results of simulations

A simulation with an initial distortion of the surface with height $d = 0.1$ near the outer edge of the tank and height zero at $r = 0$ was performed. The radius was set to be $R = 12.5$ to match the basin in the wave tank experiment [7]. This distortion propagated inward until it reached the centre, where a central wave of height approximately 50% higher than the original was generated. Figure 1 shows a surface plot of the high peak generated in the middle, at $r = 0$, due to the converging wave and it is noticeable that the surrounding waves are significantly smaller. This is already indicative that the focusing could create a wave of greater height than the surrounds.

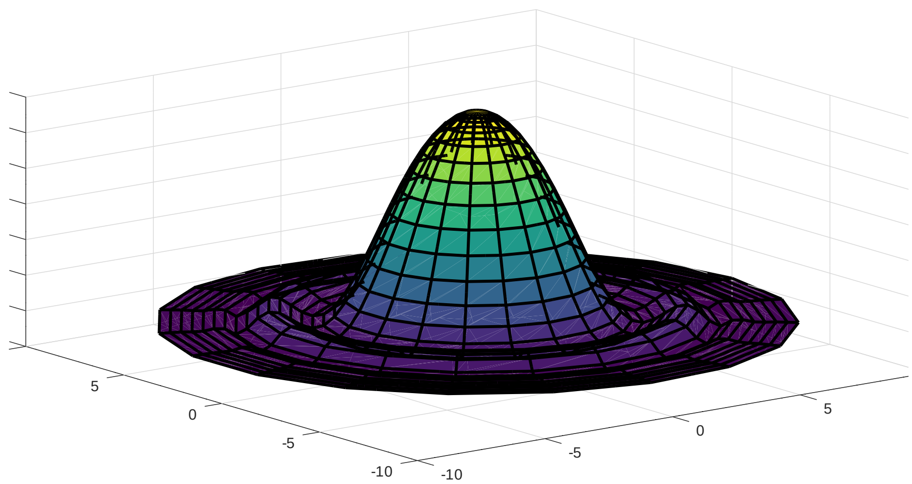

Figure 1: Surface plot of the peak wave generated by the linear solution. The central "spike" is the result of convergence of the incoming radial wave.

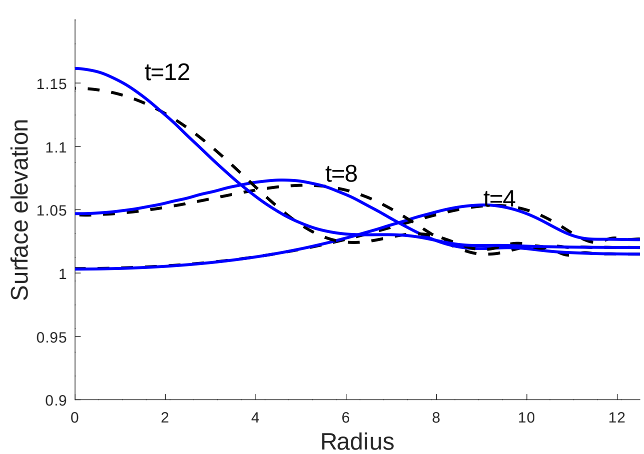

Figure 2: Comparison of linear solution (solid line) with nonlinear solution (dashed line) for the radial surface elevation at $t = 4, 8, 12$. The linear solution peaks at a slighly higher value at $r = 0$, but the agreement is good for most of the time. The nonlinear solution has slightly more wave activity.

A comparison of the linear and nonlinear solutions is shown in Figure 2 at times $t = 4$, $t = 8$ and $t = 12$. The comparison is quite good for the case of 50 coefficients in the series, with the vertical displacement of the nonlinear simulation being slightly smaller and the wave speed also being marginally smaller. These differences are consistent with the approximations inherent in the linear solution. This comparison vindicates the numerical method for the nonlinear equations. However, it is clear from the linear solution alone that a distortion of the free surface at the edge of the "tank" can lead to a higher peak in the centre of the basin. Even with a single distortion a wave 50% higher was generated. However, it is to be expected that if several waves were generated with the correct frequency then a much larger central "spike" could be generated. It is clear that a higher wave can be generated if the bottom topography can lead to the generation of incoming, circular waves to a particular location. This work verifies the possibility that the focusing of converging waves can lead to the generation of an abnormally high wave as suggested by McAllister et al [7], and suggests the possibility that a bottom topography that leads to such focusing might be the cause of some of these waves.

3 Ocean current interactions

One of the possible mechanisms for rogue waves is the interaction and subsequent associated turbulence of currents from different directions, such as the multiple currents that meet at the bottom of the African continent. While it is not possible to simulate completely the bottom topography of the region and the merging of currents, it is possible to derive some idea of the flow by considering a simplified geometry.

Assuming an ideal fluid model we considered the flow due to the three major currents in the region; the southern ocean flow from the west that diverts up to become the gulf stream, the general southern ocean circulation current and the Algulhas current that comes down the east coast of Africa. This final current comes down and around to the west before turning back to join the southern ocean current. This is an area that is very turbulent and a likely source of high wave activity. Assuming an ideal fluid, then

$$\nabla^2\Phi = 0,$$

and assuming no flow through the boundaries, in this case the coast of South Africa, we can estimate the location of the transitions from one current to another, where one might expect heightened wave activity. To avoid attempting to simulate the whole ocean circulation, we place a sink on the west coast at B to represent the gulf stream and a source at D on the east coast to represent the Agulhas current. In this very simple model we can derive the streamlines from complex variable theory. These provide an idea of the interactions between the coast and the flows.

Using complex variables it is possible to map the lower half w-plane to the lower half z-plane with a semi-circle cut out. This cut-out can represent South Africa (see Figure 3). In the w-plane the solution for the flow in complex variables is

$$f(w) = Uw + \frac{m_B}{2\pi}\ln(w - w_B) - \frac{m_D}{2\pi}\ln(w - w_B)$$

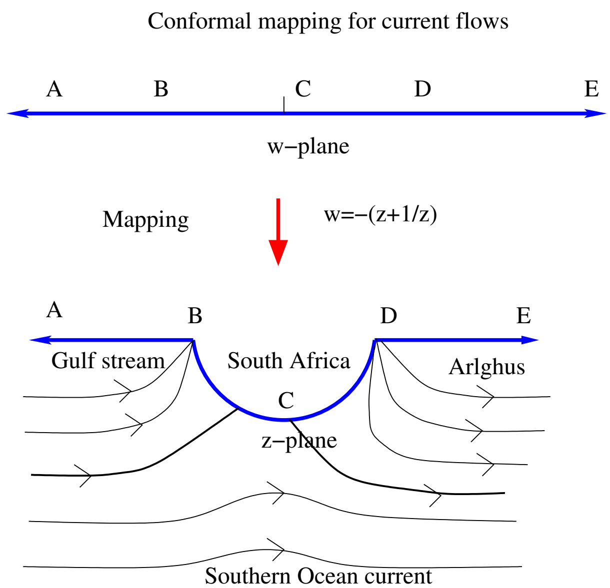

Figure 3: Mappings used in derivation of the flow currents.

which in the $z = x + iy$ physical plane is

$$f(z) = \phi + i\psi = U(z + 1/z) - \frac{m_B}{2\pi}(\ln(z + 1/z - w_B) + \frac{m_D}{2\pi}(\log(z + 1/z - w_D) \quad (27)$$

where U is the speed of the southern ocean current and m_B and m_D represent the sink and source strengths to simulate the gulf stream and Agulhas currents respectively. Varying these can simulate differing current strengths, as seen in Figure 4, which shows an example where the Agulhas current pushes further around so that the dividing line is on the west coast (top panel), while the second case (bottom panel) shows the symmetric case where the attachment to the coast is at the southern-most tip of the cape. These represent seasonal variations and knowing the locations of interaction is important in identifying potential locations of higher turbulence and waves.

This is a very approximate solution and clearly is not representative of the actual flow volumes, but a more accurate representation can be obtained by using more complicated mappings, including the location of islands and also some depth averaging to compute the flows. The behaviour of these currents and the flows can be modified to take into account the ocean bottom topography, including the continental shelf and the many islands and rocks in the region. Using these solutions, we can see a flow situation that indicates the dividing lines shown schematically in Figure 3. In this simplified model the flows are divided in such a way that the dividing streamlines appear to attach to the coast. The location of these separation points will vary as the oceanic flows vary, meaning that there will be regions where there may be some locations for which there will be rapid changes in current environment, flow and direction. The Algulhas region has the prevailing winds directly opposed to the current direction leading to the likelihood of steeper waves, and there is also interaction with the continental shelf which could generate waves in certain circumstances. More detailed data is needed to extend this model further.

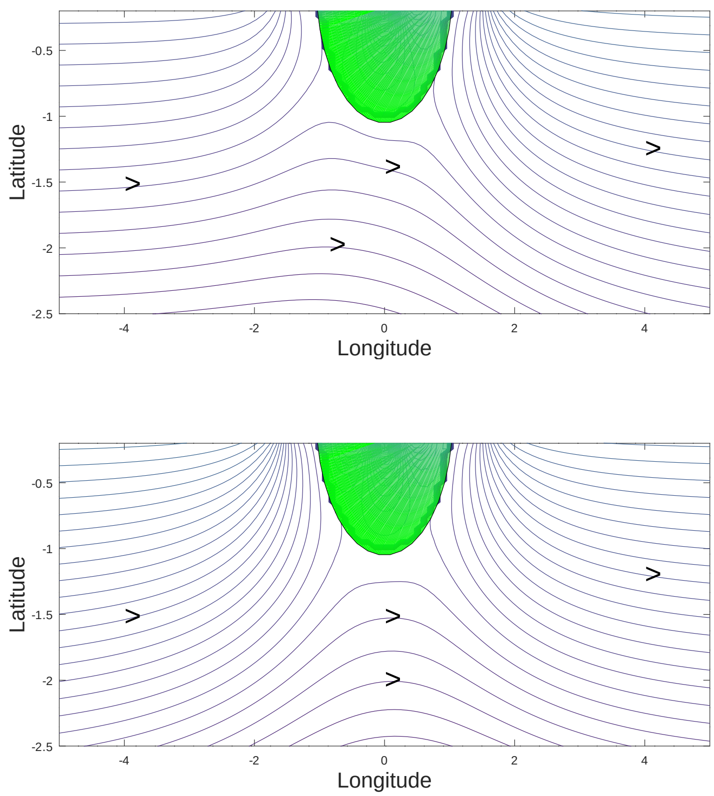

Figure 4: Examples of flow past "South Africa". In these, $U = 1$, $w_B = -w_D = 2.2$, and $m_B = 0.85, m_D = 0.45$ (top) and $m_B = 0.8, m_D = 0.8$ (bottom). In the former case the dividing streamlines attach to the coast more to the upstream (western) side, while in the latter case it is symmetric, and so attaches to the southern most point of land.

4 Data analytic approach

In the absence of local detail in the model, it is reasonable to consider a range of ocean and weather data at different coastal locations and correlate with the known occurrences of large waves. It may be possible to obtain a time series of significant wave height for each region and then work out likelihood of larger wave convergences. We note that if significant wave height is 4 m, then a "rogue" would be potentially 8 m or more, but if significant wave height is 2m, then a 4 m "rogue" is unlikely to be as serious. However we note that rogue waves have often been described as having arisen out of calm sea conditions. Using these data, it would be possible to work out how often the sea conditions might lead to a rogue wave of sufficient magnitude to cause damage, or to find a correlation between sea conditions, weather and wave occurrence, thus providing conditions under which warnings could be made.

4.1 Some real data

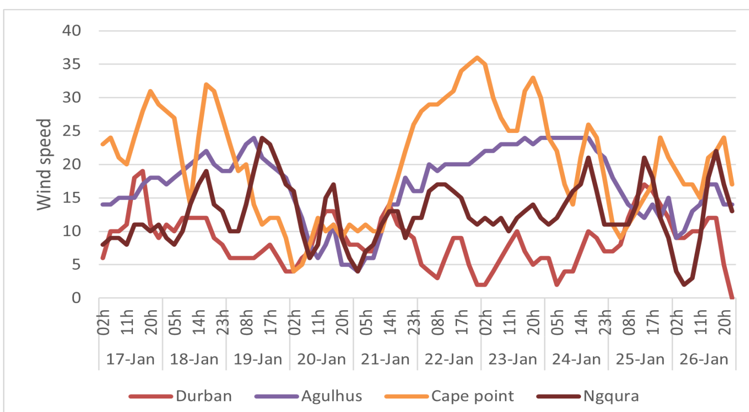

Figure 5: Wave heights and windspeed at the four ports, Cape Aghulhas, Cape Point, East London (Ngqura) and Durban over a 12 day period in January, 2024, computed from the available data.

The group was unable to obtain full data sets for an extended period, but was able to collect data from 4 locations over a 12 day period. Figure 5 shows data for the four locations, of Cape Aghulhas, Cape Point, East London (Ngqura) and Durban harbours. Wave heights and wind speed for the four ports are shown over the same period and assessment of these factors might be used to consider the major factors such as wind speed and direction and ocean current that may lead to the formation of rogue waves and the times at which they occur. Using these, it was possible to estimate the significant wave height at the four locations; Cape Agulhas (3.04), Cape Point (3.14), East London (Ngqura) (2.31) and Durban (1.91). It is clear that higher significant wave height might lead to more likelihood of a damaging rogue wave.

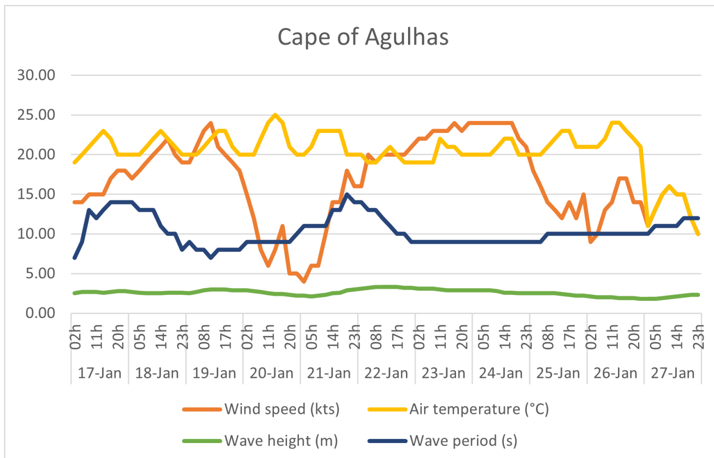

(a)

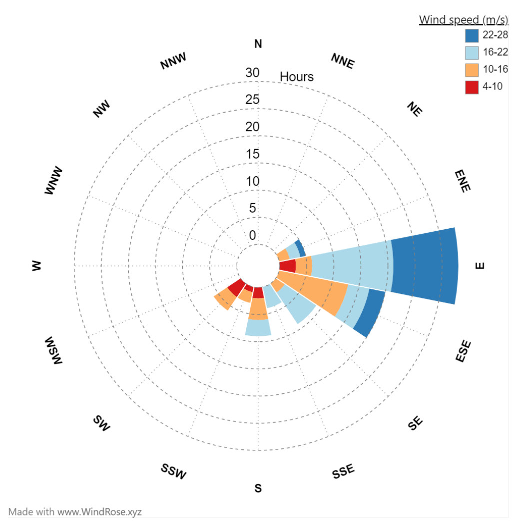

(b)

Figure 6: Port of Agulhas wind speed and direction over the period of data (upper panel), and some interpretation as a wind rose showing the magnitude and wind direction over the relevant period at the Port of Agulhas in a convenient format (lower panel).

Using this information, plots such as Figure 6 (upper panel) can be interrogated to produce plots such as Figure 6 (lower panel) which takes the data and produces a so-called "rose plot" of wind. The prevailing wind direction at the Port of Agulhas over this period, and its strength, can clearly be seen. Similar plots for other factors and statistical analyses to test for correlations between weather, sea state and topography can be used to identify conditions under which rogue waves form and propagate.

5 Final remarks

This is a very difficult problem. Trying to predict an event that is 1 in 30,000 is fraught with uncertainty and is almost certainly highly dependent on the initial conditions of any model. Therefore a simulation model would not be able to predict exact times and locations, but rather locations in which rogue waves are likely to be encountered.

We have demonstrated that we can reproduce the conditions for the formation of rogue waves by almost reproducing the Draupner Wave Tank Experiment and, in previous work [5], using the Korteweg deVries and Schrödinger equations to generate solitons for flow over bottom obstructions. However, these can not resolve all of the topography of the Southern African coast and so further work is necessary.

The group believes that a detailed analysis of sea state and weather conditions at times when rogue waves have been reported is likely to be the most fruitful in prediction and hence mitigating the damage from these events.

References

[1] M Christou and K Ewans. Field measurements of rogue water waves, *Journal of Physical Oceanography*, **44**, 2014, 2317-2335, doi: 10.1175/JPO-D-13-0199.1.

[2] L Cavaleri, A Benetazzo, F Barbariol, J Bidlot and P A E M Janssen. The Draupner event: The large wave and the emerging view. *Bull. Amer. Meteor. Soc.*, **98**,2017, 729-735, https://doi.org/10.1175/BAMS-D-15-00300.1.

[3] K B Dysthe, H E Krogstad and P Müller. "Oceanic rogue waves", *Ann. Rev. Fluid Mech.*, **40**, 2008, 287-310, doi = 10.1146/annurev.fluid.40.111406.102203

[4] R H J Grimshaw. "Transcritical flow past an obstacle", *ANZIAM J.*, **52**, 2010, 2-26, doi: 10.1017/s1446181111000599.

[5] G Hocking and C Please. "Rogue waves", Proc. MISG, 2019 African Institute for Mathematical Sciences, Muizenburg, Cape Town, January 14-18, 2019 (https://www.wits.ac.za/csam/misg/outcomes/)

[6] D J Korteweg and G de Vries. "On the change of form of long waves advancing in a rectangular canal and on a new type of long stationary waves". *Philosophical Mag.* 5th Series. **39**, 1895, 422-443, doi:10.1080/14786449508620739.

[7] M McAllister, S Draycott, T A A Adcock, P H Taylor and T S Van Den Bremer. Laboratory recreation of the Draupner wave and the role of breaking in crossing seas, *J. Fluid Mech.*, **860**, 2019, 767-786.

[8] T E Stokes G C Hocking and L K Forbes. "Steady free surface flows induced by a submerged ring source or sink", *J. Fluid Mech.*, **694**, 2012, 352-370.